ORIGINAL PAPER

Utilization of theoretical studies of the imprinting ratio to guide experimental research into the molecular imprinted polymers formed using enrofloxacin and methacrylic acid

**Junbo Liu · Zhengqiang Dai · Bo Li · Shanshan Tang ·
Ruifa Jin**

Abstract Computational approaches have been suggested as rational and fast methods for optimizing imprinting ratios. The B3LYP/6-31 g(d,p) level was applied to simulate the self-assembled system of molecularly imprinted polymers (MIPs) formed by enrofloxacin (ENRO) and methacrylic acid (MAA). Geometry optimization, the bonding situation, and the binding energies involved were studied to determine the impact of varying the imprinting ratio on the recognition characteristics. These theoretical results showed that the compound with an ENRO:MAA ratio of 1:7 had the lowest binding energy and the most stable structure. MIPs with different imprinting ratios of ENRO to MAA were then prepared in order to study the binding capacities of the polymers experimentally. The experimental and theoretically calculated results for these polymers were found to be consistent with each other. In dynamic adsorption experiments on the MIPs, the adsorption reaction was observed to reach a balanced state after 120 min. Analysis of the Scatchard plot revealed that the dissociation constant (K_d) and the apparent maximum binding capacity (Q_{max}) of MIPs with high-affinity sites were 451.67 mg/L and 42.23 mg/g, respectively, whereas the dissociation constant and apparent maximum binding capacity of MIPs with low-affinity sites were 883.39 mg/L and 73.15 mg/g, respectively. The quantity of ENRO adsorbed onto the MIPs was considerably higher than the quantities of ciprofloxacin (CIP) and ofloxacin (OFL) adsorbed, indicating that these MIPs have a much higher specific absorption capacity than the corresponding non-imprinted polymers.

Keywords Enrofloxacin · Methacrylic acid · Molecularly imprinted polymers · Computer simulation · Preparation

Introduction

Enrofloxacin (ENRO), a generic antibiotic, has been widely used in animal feed additives due to its strong broad-spectrum antibacterial properties [1]. However, because of the improper use and incomplete metabolism of ENRO by animals, ENRO residues often remain in foods derived from those animals, and the negative effects of those residues are a major threat to human health [2, 3]. Therefore, it is crucial to be able to detect ENRO residues in food analysis [4, 5]. A wide variety of methods are currently used to detect ENRO residues, such as high-performance liquid chromatography (HPLC) [6], mass spectrometry [7–9], enzyme immunoassay [10], and so on. However, it is still difficult to separate ENRO from complex sample matrices directly without applying a pretreatment process. Consequently, a clean-up step is required to improve the sensitivity and the specificity before instrumental analysis. Recently, molecularly imprinted polymers (MIPs) have been used in the food safety monitoring domain due to their unique characteristics, such as their high physical and chemical stabilities, their affinities, and their capacity to separate, purify, and enrich substances of interest in complex matrices [11–13].

The utilization of computer simulations instead of some conventional tests has greatly reduced the number of

J. Liu · Z. Dai · S. Tang (✉)
College of Resources and Environment, Jilin Agricultural University, Changchun 130118, China
e-mail: tangshanshan81@163.com

B. Li
Hebei Provincial Key Laboratory of Inorganic Nonmetallic Materials, College of Materials Science and Engineering, Hebei United University, Tangshan 063009, China

R. Jin
Department of Chemistry, Chifeng University, Chifeng 024000, China

experiments that must be performed, as well as the materials and human resources required. The guidance afforded by the results of such simulations can improve the efficiency of experiments on MIPs, as well as the affinities and selectivities of the MIPs themselves. The key to preparing MIPs with high recognition for the target molecule is optimizing the binding process of the template molecule and the functional monomer. In particular, the imprinting ratio of the template molecule to the functional monomer has a direct influence on the stability, adsorption, and selectivity of MIPs. Therefore, in order to improve these aspects of MIPs, an increasing number of researchers have unraveled the theory behind the molecular imprinting system in order to optimize the conditions employed for the synthesis of MIPs, using molecular simulations to improve the efficiency of their research into MIPs [14, 15]. ENRO MIPs are currently often prepared using methacrylic acid (MAA) as the functional monomer; in previous reports, the imprinting ratios of ENRO and MAA used were 1:4 [16], 1:6 [17], 1:8 [18, 19], and even 1:10 [11]. Gholivand et al. simulated the monomers with the highest binding scores to MIPs using the B3LYP/6-31G(d,p) method [20]. He et al. studied the stabilization energies, natural bond orbitals, and electronic density topologies of melamine and m-phelylene diamine in MIPs at the B3LYP/6-31G(d,p) level [21]. The Liu group predicted the interactions between the template atrazine and the monomers methyl methacrylate (MMA) and trifluoromethacrylic acid (TFMAA) using the B3LYP/6-31G(d,p) method [14], and the interactions between the template ciprofloxacin and the monomers MAA, 4-vinyl pyridine (4-Vpy), AAM, and TFMAA by the LC-WPBE/6-31 g(d,p) method [22]. However, there have been no reports of studies establishing molecular models for ENRO and MAA at the molecular level and simulating the imprinting interaction between them.

In the work reported in this paper, ENRO was used as the template molecule and MAA was used as the functional monomer. Calculations were performed at the B3LYP/6-31G(d,p) level of DFT using the Gaussian 09 software to determine the optimum imprinting ratio of ENRO to MAA. In addition, MIPs with different imprinting ratios of ENRO to MAA were prepared in order to study the binding capacities of the polymers experimentally. Then ENRO MIPs with the optimum imprinting ratio of ENRO to MAA (1:7) were synthesized by precipitation polymerization. The static equilibrium adsorption method was used to study the binding capacity and selectivity properties of these polymers.

Materials and methods

Materials

ENRO, ciprofloxacin (CIP), and ofloxacin (OFL) were bought from Shanghai Yuanye Biology Technology Inc.

(Shanghai, China), and the purities of these substances were over 98 %. MAA and azobisisobutyronitrile (AIBN) purchased from the Tianjin Guangfu Fine Chemical Research Institute (Tianjin, China) were recrystallized prior to use. Acetonitrile (ACN) was obtained from the Fuchen Chemical Reagent Factory (Tianjin, China). Ethylene glycol dimethacrylate (EDMA) was bought from the Shanghai Jing Pure Reagent Co., Ltd. (Shanghai, China). Methanol, acetic acid, and phosphate were products from Beijing Chemical Works (Beijing, China). All reagents used except for ENRO, CIP, and OFL were of analytical grade.

Computational approach

DFT functions [23], including B3LYP, PBE0, LC-WPBE, CAM-B3LYP, and WB97XD, were used to find the best method for optimizing the geometry of ENRO (Fig. 1) in comparison with crystal data [24]. The optimized results are presented in Table 1. The data in Table 1 show that the B3LYP method affords the most accurate geometry of ENRO (when compared with the crystal data), so the B3LYP/6-31G(d,p) method was used for all of the geometry optimizations performed during the rest of our study.

All calculations were carried out with the Gaussian 09 software using the B3LYP/6-31G(d,p) method to optimize the conformations of ENRO, MAA, and the complex, and the energies of the molecules with optimized geometries were then obtained. Natural bond orbital (NBO) charges were also calculated to predict the reactive sites. We calculated the vibrational frequencies of the optimized species at the same level and the results showed that there was no imaginary frequency. To gain additional insight into the bonding characteristics of the studied X–H···Y complexes, the atoms in molecules (AIM) theory was applied [25, 26]. The binding energies of the ENRO–MAA complexes, ΔE_B, were calculated using Eq. 1 below.

$$\Delta E_B = E_{complex} - E_{template} - \sum E_{functional\ monomer}. \qquad (1)$$
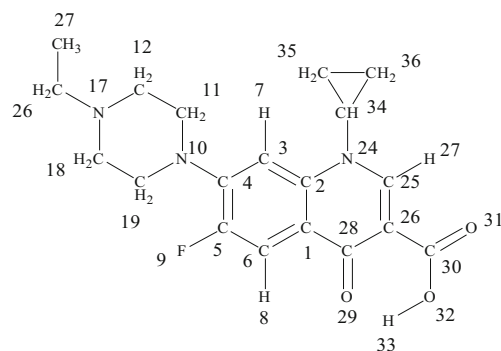

Fig. 1 Molecular structure of ENRO

Table 1 Structural parameters of ENRO calculated at the B3LYP, PBE0, LC-WPBE, CAM-B3LYP, and WB97XD levels and the corresponding available experimental data (R and Φ are the bond length and angle, respectively)

Species	B3LYP	PBE0	LC-WPBE	CAM-B3LYP	WB97XD	Expt[a]
R (nm)						
C_4–C_5	0.1422	0.1419	0.1415	0.1415	0.1418	0.1423
C_{26}–C_{25}	0.1368	0.1365	0.1357	0.1357	0.1363	0.1373
C_5–F_9	0.1354	0.1344	0.1345	0.1345	0.1344	0.1358
C_{28}–O_{29}	0.1253	0.1247	0.1241	0.1241	0.1244	0.1274
N_{24}–C_{34}	0.1452	0.1442	0.1442	0.1442	0.1445	0.1457
Φ (°)						
C_6–C_5–C_4	122.64	122.45	122.34	122.34	122.38	123.54
C_5–C_4–C_3	116.58	116.78	117.02	117.02	117.03	115.65
C_4–C_3–C_2	121.64	121.54	121.43	121.43	121.41	121.77
C_3–C_2–C_1	120.15	120.13	120.01	120.00	120.11	120.27
C_2–C_1–C_6	118.48	118.61	118.92	118.92	118.77	118.43
C_1–C_{28}–O_{29}	121.81	121.92	121.81	121.82	121.79	121.22
C_1–C_{28}–C_{26}	115.13	114.98	114.92	114.93	114.97	116.54
C_6–C_5–F_9	118.63	118.85	119.11	119.12	119.04	117.83
C_{26}–C_{28}–O_{29}	123.05	123.10	123.26	123.25	123.24	122.23
C_{25}–N_{24}–C_{34}	119.69	119.75	119.79	119.80	119.76	119.34
N_{24}–C_{34}–C_{35}	119.96	119.58	119.31	119.32	119.25	121.37
N_{24}–C_{34}–C_{36}	119.74	119.38	119.09	119.10	119.21	119.57
C_{34}–C_{36}–C_{35}	60.22	60.21	60.17	60.18	60.14	60.37
C_{25}–C_{26}–C_{30}	117.31	117.31	117.30	117.30	117.17	118.41

[a] *Expt*: experimental data from [21]

The basis set superposition error (BSSE) [27] was taken into account using the counterpoise (CP) correction method when calculating the binding energy.

Preparation and characterization of MIPs and NIPs

The ENRO MIPs were synthesized with 0.25 mmol ENRO and 1.75 mmol MAA, which were dissolved by ultrasound in 30 mL ACN. After 24 h, the crosslinker EDMA (8.75 mmol) and the initiator AIBN (50 mg) were added to the above solution. This mixture was treated with ultrasound for 30 min and then sealed under a nitrogen atmosphere for 5 min. Polymerization was performed in a water bath at 60 °C for 24 h. The resulting microspheres were collected by centrifuge. The template molecules were extracted from the product with a methanol/acetic acid (4/1, v/v) mixture by applying a Soxhlet extraction system for 48 h. Methanol was then used to remove the residual acetic acid until pH7.0 was achieved. The MIPs obtained in this manner were finally dried in a vacuum drying chamber at 50 °C for 24 h. Non-imprinted microspheres (NIPs) were also prepared for use as a blank sample using the same method except that ENRO was not added.

The MIPs and NIPs were characterized by scanning electron microscopy (SEM, JSM-6510, JEOL, Tokyo, Japan) and Fourier transform infrared spectroscopy (FTIR, Spectrum 100, PerkinElmer, Waltham, MA, USA).

Adsorption experiments

The influences of various experimental parameters such as the contact time, initial concentration, and temperature on the ability of the MIPs to adsorb ENRO were studied. To do this, 20 mg MIPs/NIPs were placed into a 50-mL Erlenmeyer flask with stopper. Then 5 mL of ENRO solution with a predefined concentration of ENRO were added to the above Erlenmeyer flask. The mixture was gently shaken at constant temperature in an oscillator for a certain period of time. This solution was filtered through a 0.22-μm membrane filter. The concentration of ENRO was determined using UV-visible absorption spectroscopy at a wavelength of 237 nm. The equilibrium adsorption capacity was calculated by performing three binding processes in succession.

The equilibrium adsorption capacity (Q, mg/g) was calculated according to Eq. 2 below, and the corresponding adsorption isotherms and kinetics curves were then obtained.

$$Q = (c_0-c)V/W \tag{2}$$

Here, c_0 (mg/L) and c (mg/L) are the initial and equilibrium concentrations of ENRO, respectively. V (mL) is the total volume of the solution and W (mg) is the weight of MIPs or NIPs. The experimental results are presented in the "Electronic supplementary material," ESM.

Selective recognition experiments

The selectivity of the MIPs for ENRO was estimated by introducing CIP and OFL as interfering agents with molecular structures that are quite similar to that of ENRO. Twenty milligrams of MIPs or NIPs were added to 5 mL of a solution of ENRO, CIP, and OFL at an initial concentration of 100 mg/L. After incubation at 28 °C for 20 h, this mixture was filtered through a 0.22-μm membrane filter. The concentrations of ENRO, CIP, and OFL in the filtrate after adsorption were measured using a UV-visible spectrophotometer. The equilibrium adsorption capacity (Q, mg/g) was calculated based on the changes in the substrate concentrations before and after absorption. The selective factor (α) was then calculated via

$$\alpha = Q_i / Q_j, \tag{3}$$

where Q_i is the adsorption capacity of MIPs or NIPs for ENRO and Q_j is the adsorption capacity of MIPs or NIPs for CIP and OFL (mg/g).

Results and discussion

Theoretical study of the imprinting ratio of template to functional monomer

The optimized structures of ENRO and MAA and the NBO charges on the proton donors and proton acceptors in ENRO and MAA are shown in Fig. 2. The figure shows that the proton donors are H_8, H_{27}, and H_{33} and the proton acceptors are F_9, O_{29}, O_{31}, and O_{32} in ENRO, based on spatial considerations. For MAA, the proton donor is H_{12} and the proton acceptor is O_{10}.

Based on NBO charge analysis of the proton donors and acceptors in ENRO and MAA, complexes with various ratios (1:1, 1:2, 1:3, 1:4, 1:5, 1:6, 1:7, and 1:8) of ENRO to MAA were simulated. The resulting optimized complex of ENRO

and MAA (for each ratio) possessed the lowest total energy of any of the complexes with that ratio of ENRO to MAA and included the maximum number of hydrogen bonds. When the imprinting ratio of ENRO to MAA was 1:8, the stability of the compound was considerably lower than the stabilities of the complexes with other imprinting ratios due to the increased distances between the template molecule and the functional monomer molecules, which were in turn caused by the limited space available for functional molecules to occupy close to the template molecule as well as the decreased amount of H-bonding between each monomer and the template. Therefore, we optimized the complexes with imprinting ratios of ENRO to MAA ranging from 1:1 to 1:7, and the optimized models with the lowest total energies are shown in Fig. 3. The models and energies of complexes with different ratios of ENRO to MAA as well as their isomers are shown in Fig. S2 of the ESM.

According to the results presented in Fig. 3, complex (1:1) includes two hydrogen bonds. The active sites associated with the hydrogen bonds (bond lengths) are $O_{31}\cdots H_{52}-O_{51}$ (0.1677 nm) and $=C_{25}-H_{27}\cdots O_{50}$ (0.2197 nm), respectively. All of the bond lengths were within the range of lengths associated with hydrogen bonds [28]. Complexes (1:2), (1:3), (1:4), (1:5), (1:6), and (1:7) include four, six, eight, nine, eleven, and twelve hydrogen bonds, respectively. As the imprinting ratio of monomer to template increases, the number of hydrogen bonds increases and the number of sites involved in interactions also increases. As a result, the strength of the interaction between ENRO and MAA decreases in the order 1:7>1:6>1:5>1:4>1:3>1:2>1:1. The structures of the template and functional monomer determine the way in which they combine. The hydrogen bonds formed between ENRO and various numbers of MAA molecules are of different degrees, and these hydrogen-bond interactions play a significant role in the formation of complexes with high stability and selectivity.

The BSSE-corrected binding energies for complexes (ΔE) are given in Table 2. From the table, it is clear that the absolute value of ΔE increases as the imprinting ratio of template to monomer increases. As shown in Fig. 3 and Table 2, the (1:7) ENRO–MAA complex had the lowest binding energy and the

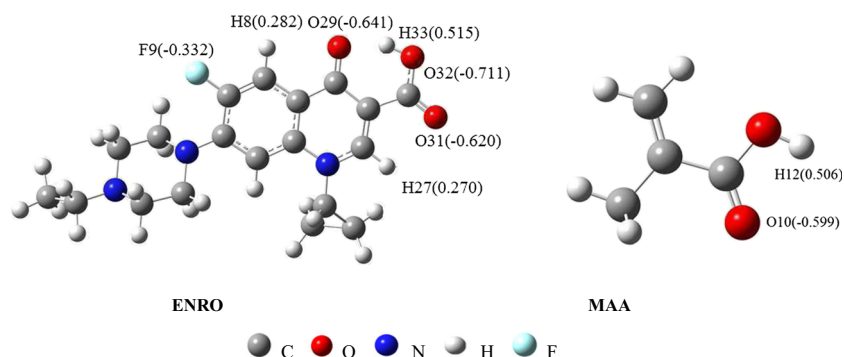**Fig. 2** Conformations of the template and the functional monomer molecules

H8(0.282) O29(-0.641) H33(0.515)
F9(-0.332)
O32(-0.711)
O31(-0.620)
H27(0.270)

H12(0.506)
O10(-0.599)

ENRO   MAA

● C   ● O   ● N   ● H   ● F

Fig. 3 Models of complexes formed from ENRO and MAA in different ratios

Complex(1:1)

Complex(1:2)

Complex(1:3)

Complex(1:4)

Complex(1:5)

Complex(1:6)
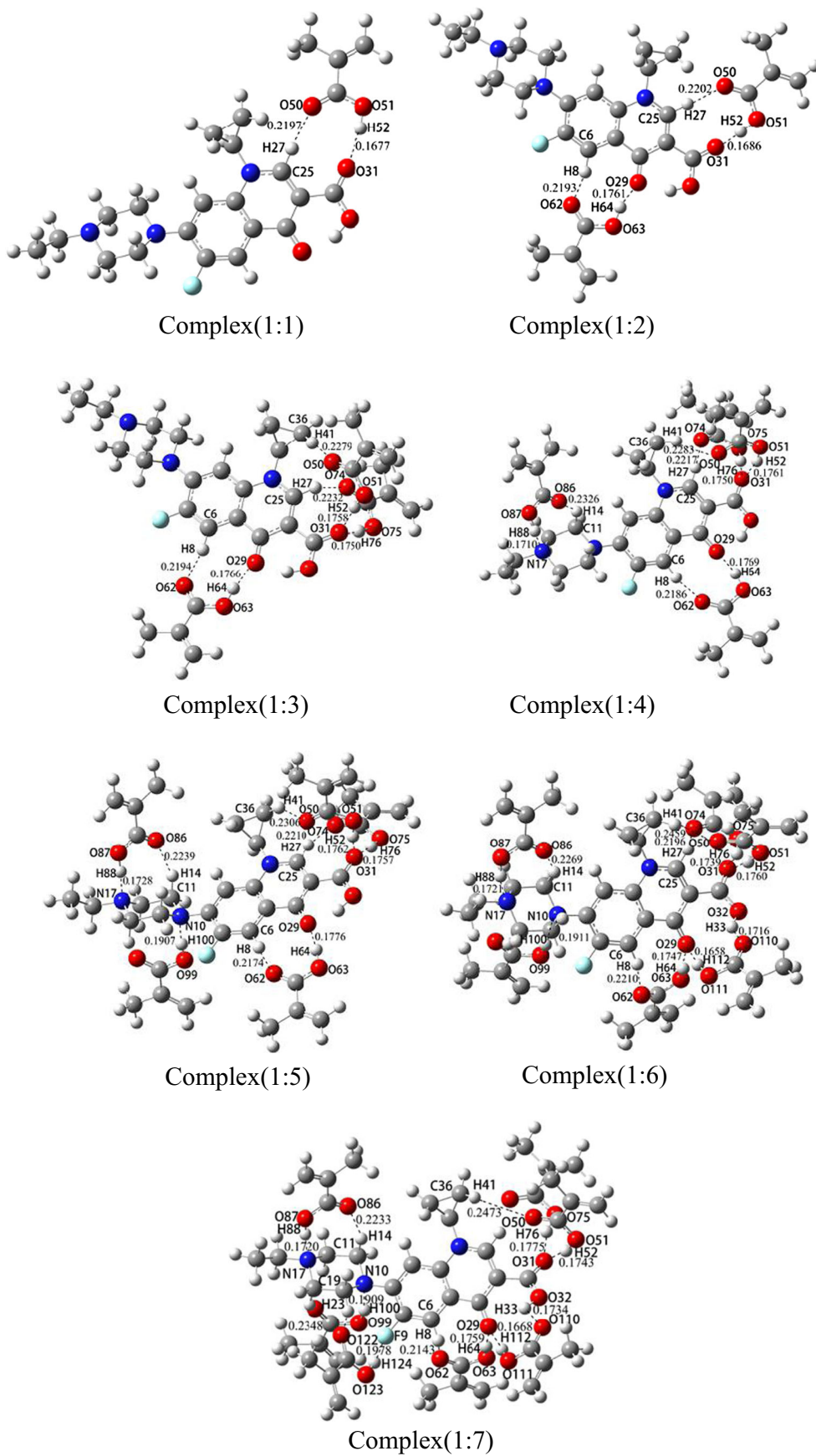
Complex(1:7)

Table 2 Binding energies (ΔE_B) of the complexes calculated at the B3LYP/6-31G(d,p) level

Species	E (kJ/mol)	ΔE_B (kJ/mol)
ENRO	−3221644.836	–
MAA	−804696.549	–
Complex(1:1)	−4026388.211	−46.826
Complex(1:2)	−4831116.458	−78.525
Complex(1:3)	−5635843.595	−109.113
Complex(1:4)	−6440576.939	−145.908
Complex(1:5)	−7245291.057	−163.477
Complex(1:6)	−8053062.161	−172.015
Complex(1:7)	−8858079.911	−186.723

Table 3 Properties of the ENRO complex (1:7) according to AIM theory (values are in au)

Active sites	$\rho(r)$	$\nabla^2\rho(r)$
$O_{31}\cdots H_{52}-O_{51}$	0.0376	0.1153
$C_{36}-H_{41}\cdots O_{50}$	0.0086	0.0307
$O_{29}\cdots H_{64}-O_{63}$	0.0359	0.1121
$C_6-H_8\cdots O_{62}$	0.0184	0.0501
$O_{31}\cdots H_{76}-O_{75}$	0.0354	0.1070
$N_{17}\cdots H_{88}-O_{87}$	0.0350	0.0953
$C_{11}-H_{14}\cdots O_{86}$	0.0166	0.0461
$N_{10}\cdots H_{100}-O_{99}$	0.0348	0.0736
$O_{29}\cdots H_{112}-O_{111}$	0.0358	0.1386
$O_{32}-H_{33}\cdots O_{110}$	0.0351	0.1208
$F_9\cdots H_{124}-O_{123}$	0.0186	0.0599
$C_{19}-H_{23}\cdots O_{122}$	0.0122	0.0367

strongest hydrogen-bond interactions, and it is the most stable. This complex includes twelve hydrogen bonds: $O_{31}\cdots H_{52}-O_{51}$, $C_{36}-H_{41}\cdots O_{50}$, $O_{29}\cdots H_{64}-O_{63}$, $C_6-H_8\cdots O_{62}$, $O_{31}\cdots H_{76}-O_{75}$, $N_{17}\cdots H_{88}-O_{87}$, $C_{11}-H_{14}\cdots O_{86}$, $N_{10}\cdots H_{100}-O_{99}$, $O_{29}\cdots H_{112}-O_{111}$, $O_{32}-H_{33}\cdots O_{110}$, $F_9\cdots H_{124}-O_{123}$, and $C_{19}-H_{23}\cdots O_{122}$, with corresponding bond lengths of 0.1743 nm, 0.2473 nm, 0.1759 nm, 0.2143 nm, 0.1775 nm, 0.1720 nm, 0.2233 nm, 0.1909 nm, 0.1668 nm, 0.1734 nm, 0.1978 nm, and 0.2348 nm, respectively. Additionally, the H-bonds strengthen the bonds between the template molecule and the functional monomer molecules. The imprinting ratio has an enormous influence on the recognition ability of the MIPs. It is well known that a higher ratio means more H-bonds, which increases the binding energy as well as the regular space pattern between the functional molecule and the template; consequently, the selectivity of MIPs for the template molecule is enhanced. These results suggest that MIPs with excellent selectivity and affinity for ENRO can be prepared by applying an imprinting ratio of ENRO to MAA of 1:7.

Polymerization of the complexes

All of the results of the analysis discussed above indicate that template molecules interact with monomer molecules through hydrogen bonds and form stable complexes. In order to reveal the role that active sites in the cavity of the MIP play in the imprinting process of MIPs, we simulated the interactions between template and monomers using the Multiwfn 3 software package [29], which is based on the AIM theory [30]. Bond critical points (BPCs) were used to estimate interactions between adjacent atoms and the BCPs connected with two atoms, respectively. At the same time, the values of their electron densities $\rho(r)_{bcp}$ and Laplacians $\nabla^2\rho(r)_{bcp}$ were used to determine the type of interaction force involved. The results of this work are shown in Table 3. As seen in Table 3, the maximum value of $\rho(r)$ was 0.0376 au, whereas the minimum value was 0.0086 au. $\nabla^2\rho(r)$ was found to be in the range

0.0307~0.1386 au. The calculated hydrogen bonds all complied with the criteria proposed by Popelier and Bader [31], i.e., $\rho(r)$ and $\nabla^2\rho(r)$ were in the ranges 0.002~0.035 au and 0.024~0.139 au, respectively. The results obtained upon applying AIM showed that ENRO interacts with MAA through hydrogen-bond interactions.

Rebinding properties

The process in which ENRO MIPs (re)bind to ENRO or its analogs was simulated in order to predict the selectivities of the ENRO MIPs. As can be seen in Table 4, the ENRO MIPs were indeed able to (re)bind ENRO or its analogs. The analogs were also able to bind to the MIPs because some of the active groups in the the molecular structures of ENRO (Fig. 4a), CIP (Fig. 4b), and OFL (Fig. 4c) are the same, and the positions of those active groups are also the same in those molecules. These results indicate that CIP and OFL fit perfectly into the imprinted cavities of ENRO MIPs. While the fluoroquinolone groups of CIP and OFL differ from that of ENRO, the rebinding energy of the ENRO MIPs with CIP or OFL was lower than that of the ENRO MIPs with ENRO. Therefore, the ENRO MIPs show the highest affinity for ENRO, the next strongest affinity for CIP, and the lowest affinity for OFL. The selectivity of ENRO MIPs for ENRO is excellent when ENRO, CIP, and OFL are all present.

Table 4 Rebinding energies of the complexes formed from ENRO and its analogs

Species	E (kJ/mol)	ΔE (kJ/mol)
Complex(ENRO)	−8854707.330	−186.652
Complex(CIP)	−8648269.573	−191.060
Complex(OFL)	−8949028.628	−175.857

Fig. 4a–c Conformations of ENRO (a), CIP (b), and OFL (c)
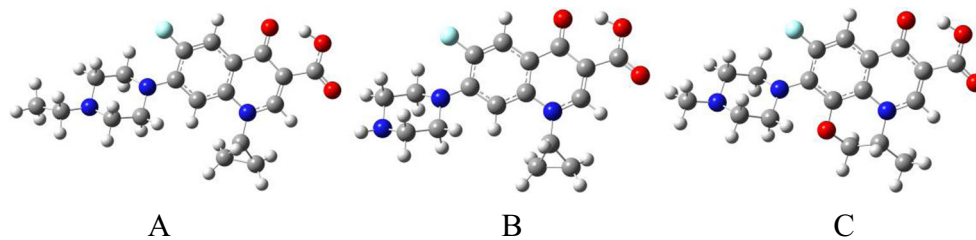
Experimental results for adsorption onto MIPs with different imprinting ratios
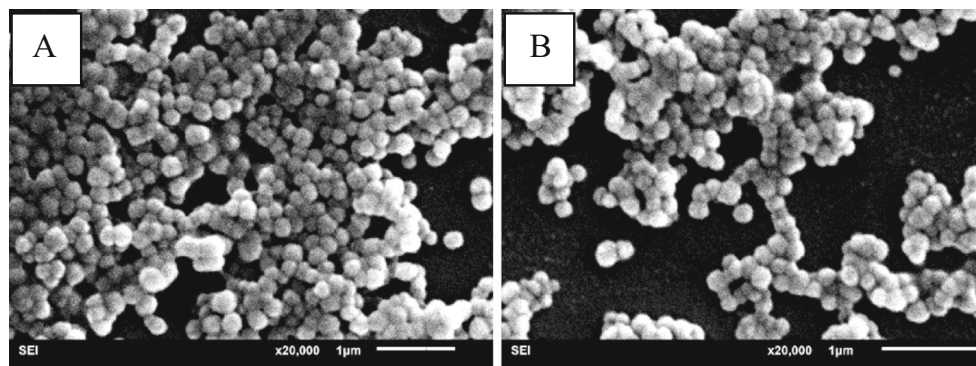
To verify the accuracy of the computer simulations, MIPs with different imprinting ratios of ENRO to MAA were prepared in order to study their binding capacities experimentally. According to the results presented in Table 5, the MIPs synthesized from ENRO and MAA in the ratio 1:7 showed the highest adsorption capacity. The experimental results were therefore consistent with the corresponding calculated results. This means that quantum chemistry can be used to predict the optimal imprinting ratio for these MIPs.

SEM analysis

SEM images of the MIP and NIP particles were obtained in order to observe the surface morphologies and particle diameters of the NIPs and the MIPs with an imprinting ratio of ENRO to MAA of 1:7; these images are shown in Fig. 5. From Fig. 5, it is clear that the MIP and NIP particles are roughly uniform, ball-like microspheres. The average particle diameter of the MIPs is 210 nm, which is greater than the average particle diameter of the NIPs (170 nm). This is because each MIP contains a cavity that can accommodate an

Table 5 Adsorption capacities of ENRO MIPs with different imprinting ratios

Imprinting ratio	1:1	1:2	1:3	1:4	1:5	1:6	1:7	1:8
Q (mg/g)	1.45	2.15	3.06	4.16	4.79	5.42	6.37	5.77

ENRO molecule, whereas each NIP does not, so each MIP needs to be larger than each NIP.

IR analysis

The IR spectra of the polymers provide structural information about them. Due to H-bond formation between the C=O group of MMA and the O–H group of ENRO, the stretching vibrations of C=O and O–H are redshifted. As seen in Fig. 6, the IR spectra of the MIPs and NIPs are similar, but the locations, widths, and strengths of the vibrational peaks for the C=O and O–H groups in MAA are significantly different. The peak at 1740 cm^{-1} for C=O in non-H-bonded MMA moves to 1729 cm^{-1} upon adding an ENRO (template) molecule, which indicates that H-bonds form between these molecules (Fig. 3). Additionally, a comparison between the stretching peak (−OH) at 3450 cm^{-1} for NIPs and that at 3436 cm^{-1} for MIPs indicates that H-bonds are present between the –OH group of MMA and the C=O group of ENRO, which is also suggested by calculations.

Adsorption kinetics analysis

The adsorption kinetics profile was obtained in ENRO solution at an initial concentration of 100 mg/L. As shown in Fig. 7, there are two steps in the adsorption process. The adsorption rate in the first 50 min is greater than the subsequent rate. The adsorption equilibrium for the MIPs had almost been reached after about 120 min. This shows that ENRO MIPs, with their numerous specific cavities for recognizing a template molecule based on shape, size, and
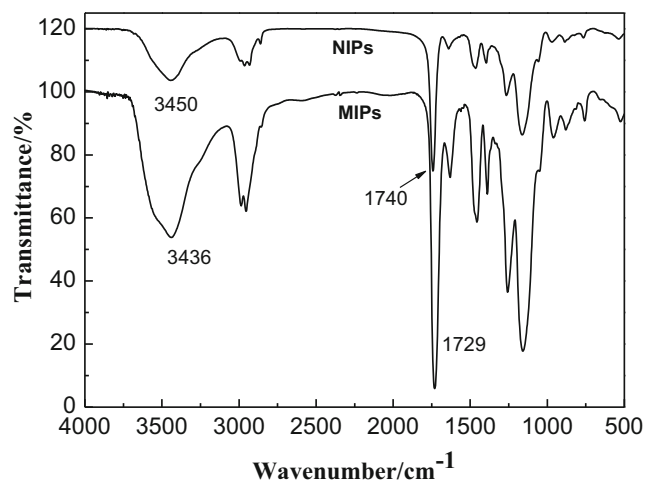
Fig. 5a–b SEM images of MIPs (a) and NIPs (b)

Fig. 6 IR spectra of MIPs and NIPs

Fig. 8 Adsorption isotherm of MIPs and NIPs

functional groups, are able to recognize a specific molecule—ENRO—and show high binding affinity for it. This high affinity can mainly be attributed to the hydrogen-bond interactions between the MIPs and ENRO molecules.

Adsorption isotherm and Scatchard plot

In order to elucidate the effects of varying the initial concentration of ENRO on the adsorption performance of NIPs and MIPs with an imprinting ratio of ENRO to MAA of 1:7, the adsorption isotherm was measured at room temperature for 120 min. Such adsorption isotherm experiments were performed in ENRO solutions with initial concentrations ranging from 20 mg/L to 800 mg/L. As shown in Fig. 8, the quantity adsorbed increased with the initial concentration of ENRO, and saturation of the MIPs and NIPs occurred at an ENRO concentration of 600 mg/L.
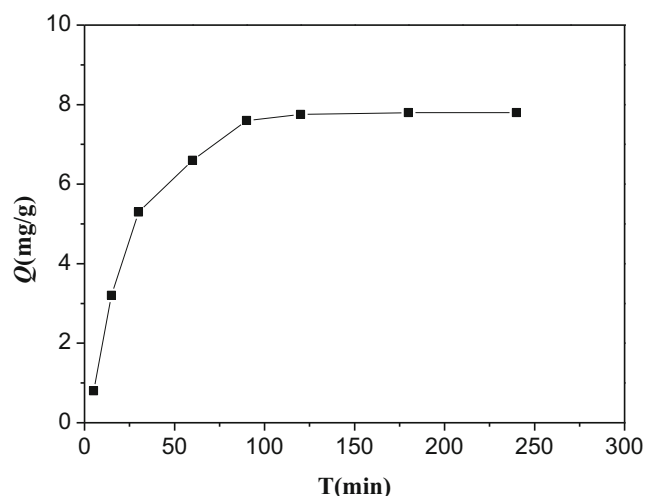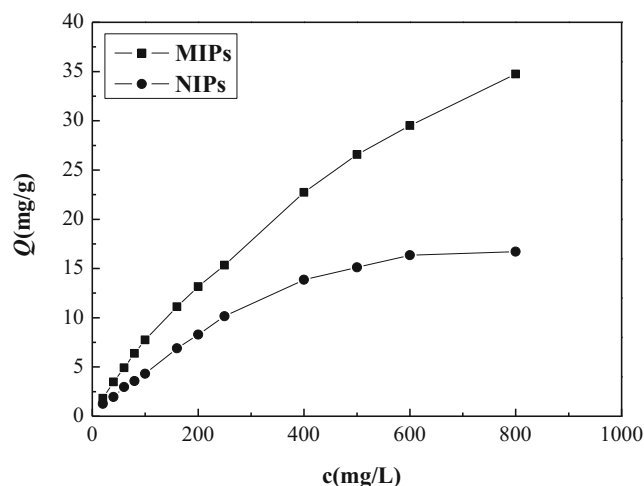
The saturated adsorption capacity of the MIPs was found to be 29.52 mg/g, which was much greater than that of NIPs (16.35 mg/g). The amount of ENRO adsorbed onto MIPs is thus higher than the amount of ENRO adsorbed onto NIPs. This is because there are a large number of ENRO-imprinted cavities in the MIPs, meaning that the MIPs have a higher affinity, better specific recognition, and a greater adsorption rate than NIPs for ENRO. Scatchard plots of MIPs were constructed via the equation

$$Q/c = (Q_{max} - Q)/K_d, \tag{4}$$

where Q (mg/g) is the quantity of ENRO adsorbed onto MIPs, c (mg/L) is the equilibrium concentration of ENRO, Q_{max} (mg/g) is the apparent maximum amount adsorbed, and K_d (mg/L) is the dissociation constant. Q/c is plotted versus Q in Fig. 9. The data in this Scatchard plot can be fitted with two linear trend lines that are given by the following equations: $Q/$
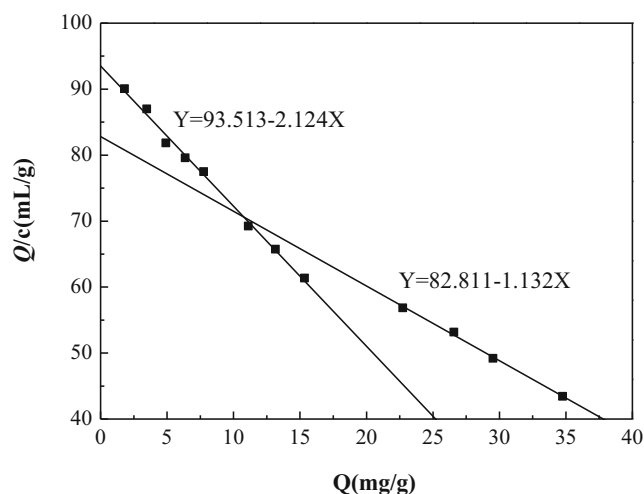

Fig. 7 Adsorption kinetics curves of MIPs

Fig. 9 Scatchard plot for the MIPs

Table 6 Q and α values for the MIPs and NIPs

Substrate	MIPs		NIPs	
	Q (mg/g)	α (MIPs)	Q (mg/g)	α (NIPs)
ENRO	6.37	–	3.56	–
CIP	4.93	1.29	2.97	1.19
OFL	4.19	1.52	2.58	1.37

$c = 93.513 - 2.124Q$ and $Q/c = 82.811 - 1.132Q$. The presence of two trend lines implies that the MIPs contain two binding sites (low- and high-affinity sites). The dissociation constant (K_d) and the apparent maximum binding capacity (Q_{max}) of the MIPs with high-affinity sites are 451.67 mg/L and 42.23 mg/g, respectively, whereas the dissociation constant and the apparent maximum binding capacity of the MIPs with low-affinity sites are 883.39 mg/L and 73.15 mg/g, respectively. These results also reveal that the imprinted polymers have high binding association constants.

Study of adsorption selectivity

In order to evaluate the adsorption selectivities of the MIPs and NIPs for ENRO, we tested the quantities (Q) of ENRO, CIP, and OFL adsorbed by the MIPs after the initial elution of ENRO as well as by the NIPs via static equilibrium adsorption. The selective factors (α) of the MIPs and NIPs were calculated using Eq. 3. The results are listed in Table 6.

From the data in Table 6, it is clear that the MIPs can adsorb certain quantities of ENRO, CIP, and OFL, and that the Q value of the MIPs for ENRO is obviously greater than those of the MIPs for CIP and OFL, respectively. The Q values of the NIPs for ENRO, CIP, and OFL are similar. This can be explained by the good match between the ENRO molecules and the cavities in MIP molecules in terms of shape, size, and functional groups, as well as the formation of stable and regular voids, whereas the NIPs show some degree of general adsorption of ENRO, CIP, and OFL but lack the features mentioned above that lead to the high affinity of ENRO for the MIPs. Table 6 indicates that the Q value of the MIPs for ENRO is 6.37 mg/g, which is larger than the corresponding values for CIP and OFL, while the Q values of the NIPs for the three compounds are all relatively similar, which proves that the NIPs have poor selectivity. These experimental results are in good agreement with the computational results for rebinding properties.

Conclusion

The present study elucidated the imprinting ratio, the nature of the imprinting, and the interaction mechanism by simulating geometry optimization, the bonding situation, and the binding energies of ENRO with different numbers of MAA molecules via quantum chemistry calculations. The results of these simulations were intended to guide the direction of experimental research in this field. Meanwhile, the accuracy of the theoretical calculations was verified by experiment. MIPs with the optimal imprinting ratio (1:7) were obtained by precipitation polymerization and found to have high adsorption specificity for ENRO. The imprinted polymers presented high binding association constants and a saturated adsorption capacity of 29.52 mg/g at an ENRO concentration of 600 mg/L. In addition, the adsorption reaction was observed to be a spontaneous exothermic process. This study provides theoretical and experimental reference information that should prove useful in the selective separation, enrichment, and detection of ENRO in a complex food matrix.

References

1. Martinez M, McDermott P, Walker R (2006) Vet J 172:10–28
2. Kalpana S, Aggarwal M, Rao GS, Environ JK (2012) Toxicol Pharmacol 33:121–126
3. Chen TT, Yuan J, Feng X, Wei H, Hua W (2011) Int J Antimicrob 37:567–571
4. Choi JH, Mamun MIR, Abd El-Aty AM, Park JH, Shin EH, Park JY (2011) Food Chem 127:1878–1883
5. Bilandžić N, Kolanović BS, Varenina I, Scortichini G, Annunziata L, Brstilo M (2011) Food Control 22:1941–1948
6. Idowu OR, Peggins JO (2004) J Pharm Biomed Anal 35:143–153
7. Tian HZ (2011) Chemosphere 83:349–355
8. Krebber R, Hoffend FJ, Ruttmann F (2009) Anal Chim Acta 637:208–213
9. Seifrtová M, Nováková L, Lino C, Pena A, Solich P (2009) Anal Chim Acta 649:158–179
10. Yu F, Wu YJ, Yu SC, Zhang HL, Zhang HQ, Qu LB (2012) Spectrochim Acta A 93:164–168
11. Li XX, Bai LH, Wang H, Wang J, Huang YP, Liu ZS (2012) J Chromatogr A 1251:141–147
12. Xu ZX, Gao HJ, Zhang LM, Chen XQ, Qiao XG (2012) J Food Sci 76:69–75
13. Puoci F, Iemma F, Cirillo G, Curcio M, Parisi OI, Spizzirri UG (2009) Eur Polym J 45:1634–1640
14. Liu JB, Sun JN, Tang SS, Chen KY, Jin RF (2012) Chin J Struct Chem 31:1794–1802
15. Dourado EMA, Herdes C, Tassel PRV, Sarkisov L (2011) Int J Mol Sci 12:4781–4804
16. Lu YK, Liu Y, Bian C, Lu GD, Qin XY (2009) CJI 1:126
17. Wang XY, Tan HR, Qi KZ, Shao L, Li H, Xue XH (2010) Chin J Chromatogr 28:1107–1110
18. Caro E, Marće RM, Cormack PAG, Sherrington DC, Borrull F (2006) Anal Chim Acta 562:145–151

19. Ton XA, Acha V, Haupt K, Bui BTS (2012) Biosens Bioelectron 36: 22–28
20. Gholivand MB, Khodadadian M (2011) Talanta 85:1680–1688
21. He Q, Zhao HL, Su GX (2014) Acta Sci Nat Univ Nankaiensis (Nat Sci Ed) 47:99–107
22. Liu JB, Sun JN, Tang SS, Jin RF (2013) Chin J Struct Chem 32: 1204–1210
23. Acelas NY, Mejia SM, Mondragón F, Flórez E (2013) Comput Theor Chem 1005:16–24
24. Jasinski JP, Butcher RJ, Siddegowda MS, Yathirajan HS, Siddaraju BP (2011) Acta Crystallogr 67:432–433
25. Bader RFW (1998) J Phys Chem A 102:7314–7323
26. Biegler-König F (2000) AIM2000. F. Biegler-König, University of Applied Sciences, Bielefeld
27. Singh RN, Kumar A, Tiwari RK, Rawat P, Gupta VP (2013) J Mol Struct 1035:427–440
28. Needham P (2013) Stud Hist Philos Sci A 44:51–65
29. Lu T (2012) Multiwfn: multifunctional wavefunction analyzer, v.2.3.1. T. Lu, Beijing Kein Research Center for Natural Sciences, Beijing
30. Bader RFW (1990) Atoms in molecules: a quantum theory. Oxford University Press, Oxford
31. Popelier PLA, Bader RFW (1992) Chem Phys Lett 189: 542–548